ResearchGate

See discussions, stats, and author profiles for this publication at: https://www.researchgate.net/publication/6932497

Can the Light Scattering Depolarization Ratio of Small Particles Be Greater Than 1/3?

ARTICLE *in* THE JOURNAL OF PHYSICAL CHEMISTRY B · JULY 2005

Impact Factor: 3.3 · DOI: 10.1021/jp0521095 · Source: PubMed

CITATIONS
51

READS
128

7 AUTHORS, INCLUDING:

Nikolai G. Khlebtsov
Institute of Biochemistry and Physiology of P…
229 PUBLICATIONS **4,814** CITATIONS
SEE PROFILE

Vladimir Aleksandrovich Bogatyrev
Russian Academy of Sciences
87 PUBLICATIONS **1,157** CITATIONS
SEE PROFILE

Lev Dykman
Saratov State University
105 PUBLICATIONS **2,390** CITATIONS
SEE PROFILE

Boris Khlebtsov
Russian Academy of Sciences
152 PUBLICATIONS **2,185** CITATIONS
SEE PROFILE

Available from: Boris Khlebtsov
Retrieved on: 26 January 2016

Can the Light Scattering Depolarization Ratio of Small Particles Be Greater Than 1/3?

Nikolai G. Khlebtsov,*,†,‡ Andrei G. Melnikov,† Vladimir A. Bogatyrev,†,‡ Lev A. Dykman,† Anna V. Alekseeva,† Lyubov A. Trachuk,† and Boris N. Khlebtsov†

Institute of Biochemistry and Physiology of Plants and Microorganisms, Russian Academy of Sciences, 13 Pr. Entuziastov, Saratov 410049, Russia, and Saratov State University, 83 Astrakhanskaya St., Saratov 410026, Russia

Received: April 22, 2005; In Final Form: May 20, 2005

According to the theory of light scattering by small randomly oriented particles (van de Hulst, H. C. *Light Scattering by Small Particles*; Wiley: New York, 1957; Kerker, M. *The Scattering of Light and Other Electromagnetic Radiation*; Academic Press: New York, 1969), the depolarized ratio of the scattered intensities, I_{vh}/I_{vv}, cannot exceed 1/3. Here we show that this conclusion does not hold for nonspherical plasmon resonant metal particles. Our analysis is based on the Rayleigh approximation and the exact T-matrix method as applied to spheroids and circular cylinders with semispherical ends. For small particles, the condition $I_{vh}/I_{vv} > 1/3$ can be satisfied within the upper left quadrant of the complex relative dielectric permeability Real(eps) < -2 (rods) and within the upper unit semicircle centered at Real(eps) $= -1$ (disks). For gold nanorods with the axis ratio exceeding 2, the maximal theoretical values I_{vh}/I_{vv} lie between 1/3 and 3/4 at wavelengths of 550−650 nm. The extinction and static light scattering spectra (450−850 nm, at 90° degrees) as well as the depolarized ratio of He−Ne laser light scattering were measured with gold nanospheres (the average diameters of 21, 29, and 46 nm) and nanorods (the longitudinal plasmon resonance peak positions at 655, 692, and 900 nm). The measured depolarization ratios of nanospheres (0.07−0.16) and nanorods (0.3−0.48) are in good agreement with theoretical calculations based on estimations of the average particle size and shape.

1. Introduction

The change in light polarization due to scattering is well known since the pioneering works of Rayleigh.[1,2] If the incident light is vertically polarized with respect to the scattering plane, the scattered light is, in general, partially (elliptically) polarized and there is nonzero scattered intensity with horizontal polarization in the scattering plane. From an experimental point of view, the cross-polarized scattered intensity I_{vh} can be conveniently characterized by the "depolarization factor"[3] or "depolarization ratio,"[4] $\Delta_{vh} = I_{vh}/I_{vv}$, where the subscripts v and h stand for vertical and horizontal polarization with respect to the scattering plane. The first and second subscripts designate the incident and scattered light polarizations, respectively. If particles are illuminated by natural (unpolarized) light, the depolarization ratio is defined[3,4] as $\Delta_{uh} = I_{uh}/I_{uv}$. Generally, the polarization of scattered light can be characterized by Stokes parameters.[3,5,6] The depolarization of light due to scattering by randomly oriented or aligned particles has been reviewed in chapter 10 of Kerker's book[4] and in refs 7−10.

According to the theory of light scattering by small particles,[3,4] the maximal value of depolarization ratio Δ_{vh} cannot exceed 1/3 and 1/8 for "usual" dielectric rods and disks with positive values of real and imaginary parts of dielectric permeability. However, we found an important exception to the above rule, which was confirmed by theoretical calculations and experimental measurements. It is a question concerning gold or silver nanorods (NRs) possessing plasmon resonances.[11−13] These nanoparticles have unique optical properties[14−16] and shows promise for nanotechnological applications.[17−20] When the light is scattered by a gold NR, it is strongly polarized along its major axis.[21]

In this work we give a theoretical analysis of the depolarization ratio for gold nanoparticles by using the Rayleigh approximation and the exact T-matrix method.[6,15] Our analysis elucidates the conditions corresponding-to-depolarization ratio values $\Delta_{vh} > 1/3$. For experimental verification of the theory, we prepared gold nanospheres with average diameters of 21, 29, and 46 nm and gold NRs with thickness of about 15 nm and axial ratios ranging from 2.5 to 4.9 (according to the longitudinal plasmon resonance extinction peak positions and to TEM data). The measured depolarization ratios for wavelengths 632.8 and 740 nm and the scattering angle $\theta = 90°$ are in agreement with the T-matrix calculations.

2. Theoretical Basis

For anisotropic randomly oriented Rayleigh particles, the depolarization ratio can be expressed through *A* and *B* invariants of the polarizability tensor[3] ($\alpha_1,\alpha_2,\alpha_3$):

$$\Delta_{vh} = \frac{A - B}{3A + 2B} \tag{1}$$

$$A = \sum_{i=1}^{3} |\alpha_i|^2,\ B = \mathrm{Re} \sum_{\substack{i,j=1 \\ i \neq j}}^{3} \alpha_i^* \alpha_j \tag{2}$$

According to estimations by van de Hulst[3] and Kerker,[4] the maximal value of the depolarization ratio Δ_{vh} cannot exceed 1/3 for rods with polarizability tensor (α,0,0) and 1/8 for disks with tensor (0,α,α).[4] The corresponding values of Δ_{uh} are equal

* Corresponding author. E-mail: khlebtsov@ibppm.sgu.ru
† Russian Academy of Sciences.
‡ Saratov State University.

10.1021/jp0521095 CCC: $30.25 © 2005 American Chemical Society
Published on Web 06/23/2005

to 1/2 and 2/9, respectively.[4] However, in section 5.3 of Bohren and Huffman's book[5] the extreme values of invariant $M = B/A = 1$ and $-1/2$ are pointed out. If we rewrite eq 1 in terms of invariant M,

$$\Delta_{vh} = \frac{1 - M}{3 + 2M} \tag{3}$$

then two Δ_{vh} limits, 0 and 3/4, are expected for the above $M = 1, -1/2$ extrema, respectively. The upper limit 3/4 exceeds essentially the limit 1/3 pointed out by van de Hulst[3] and Kerker.[4] It is evident that this discrepancy is related to the different assumptions as to the particle polarizability tensor. For "usual" molecules[4] and particles,[3,5] the values of invariant $M \geq 0$; therefore, the maximal values of the depolarization ratio cannot exceed $\Delta_{vh} \leq 1/3$. However, these estimations may not hold for metal NRs near their plasmon resonance band.

Before we consider light scattering depolarization by metal nanoparticles, let us recall a general result of the light scattering theory as applied to the incident plane wave $\mathbf{e}_0 \exp(i\mathbf{k}_0\mathbf{r})$ and to randomly oriented molecules.[22] In the general case of molecular scattering, the scattered intensity consists of three parts called *scalar*, *symmetrical*, and *antisymmetrical scattering*[22]

$$I = I^{(0)} + I^{(s)} + I^{(a)} = I_0^{(0)}|\mathbf{e}_s^*\mathbf{e}_0|^2 + I_0^{(s)}\left[1 + \left|\mathbf{e}_s\mathbf{e}_0\right|^2 - \frac{2}{3}\left|\mathbf{e}_s^*\mathbf{e}_0\right|^2\right] + I_0^{(a)}[1 - |\mathbf{e}_s\mathbf{e}_0|^2] \tag{4}$$

where the unit vector $\mathbf{e}_s$ determines the scattered light polarization, whereas constants $I_0^{(0)}$, $I_0^{(s)}$, $I_0^{(a)}$ are expressed through bilinear combinations of the polarizability tensor averaged over random orientations.[22] For scalar scattering, there is no depolarization and $I_{vh}^{(0)} = 0$. In the case of symmetrical scattering, the depolarization ratio $\Delta_{vh}^{(s)}$ does not depend on the scattering angle in the plane $(\mathbf{k}_0,\mathbf{k}_s)$ and, as it is evident from eq 4, we have $\Delta_{vh}^{(s)} = 3/4$. Finally, for antisymmetrical scattering in the plane $(\mathbf{k}_0,\mathbf{k}_s)$, the scattering intensity $I_{vv}^{(a)} = 0$. Therefore, the theoretical depolarization ratio is equal to infinity. Of course, the actual depolarization ratio is of limited practical value. We will see below that the case of metal NRs corresponds to a combination of scalar and symmetrical scattering, so the maximal depolarization ratio will be equal to 3/4.

Consider first small metal nanoparticles obeying the Rayleigh approximation. The depolarization ratios are then related by the equation $\Delta_{vh} = \Delta_{uh}/(2 - \Delta_{uh})$, so we need only Δ_{vh}. It follows from eq 1 that the condition $\Delta_{vh} \geq 1/3$ is equivalent to the condition $B \leq 0$, which has to be studied. A convenient analytical model is a spheroid with semiaxes (a,b,b), where $a \geq b$ for prolate particles and $a \leq b$ for oblate particles. For axial particles $(\alpha_1 \neq \alpha_2 = \alpha_3)$, the condition $B \leq 0$ is reduced to the inequality

$$|1 + \frac{\alpha_2}{\alpha_1}|^2 \leq 1 \tag{5}$$

Here, let $\epsilon(\lambda)$ be the particle relative dielectric permeability, which includes the size-limiting effects for conductivity electrons.[23] The principal values of the spheroid polarizability tensor are defined by the equation[3,5]

$$\alpha_i = \frac{ab^2}{3}\frac{\epsilon - 1}{1 + L_i(\epsilon - 1)} \tag{6}$$

where L_i, $i = a,b$ are the geometrical depolarization factors depending on the axial particle ratio $e = a/b$. Condition 5, then, leads to the inequality

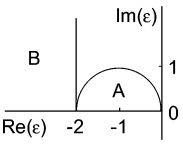

Figure 1. Complex plane of the relative dielectric permeability ϵ and the fields A and B corresponding to the depolarization ratio $\Delta_{vh} > 1/3$ for randomly oriented spheroidal disks (A) and thin rods (B).

$$|1 + \frac{1 + L_1(\epsilon - 1)}{1 + L_2(\epsilon - 1)}|^2 \leq 1 \tag{7}$$

which defines the relation between the shape and the polarizability of particles whose depolarization ratio is greater than 1/3 ($\Delta_{vh} \geq 1/3$). Let us consider two limiting cases: (1) thin disks ($a \ll b$, $e \ll 1$) and thin needles $a \gg b$,$e \gg 1$. In the first case we have $L_a = 1$, $L_b = 0$, so inequality 7 reduces to the condition

$$|1 + \epsilon|^2 \leq 1 \tag{8}$$

As $\mathrm{Im}(\epsilon) \geq 0$, we conclude that the corresponding range of ϵ is within the upper unit semicircle centered at $(-1,0)$ (Figure 1, A). For thin rods $L_a = 0$, $L_b = 1/2$, so it follows from eq 7 that

$$|\epsilon + 3|^2 \leq |\epsilon - 1|^2 \tag{9}$$

A simple analysis shows that the tolerance range of ϵ is within the upper left quadrant (Figure 1, B)

$$\mathrm{Re}(\epsilon) \leq -2, \mathrm{Im}(\epsilon) \geq 0 \tag{10}$$

For small metal spheres, the condition of plasmon resonance reads[5]

$$\epsilon(\lambda) = -2 \tag{11}$$

Considering the behavior of gold dielectric permeability in the region $\lambda \geq 520$ nm, we conclude that the condition 10 may be satisfied in the red part of the spectrum. An interesting result can be derived from eq 5 with the condition $\mathrm{Re}(\epsilon) = -2 + \delta(\delta \rightarrow 0)$, corresponding to the plasmon resonance (eq 11): the principal values of the polarizability tensor are then related by the equation $\alpha_2 = -2\alpha_1$, the invariant $B = 0$, and the depolarization ratio Δ_{vh} is equal to 1/3 irrespective of the particle aspect ratio $e \neq 1$.

The maximum possible value of $\Delta_{vh} = 3/4$ can be obtained for a polarizability tensor of the type $(\alpha, -\alpha, 0)$ or $(\alpha, 0, -\alpha)$. In the general case of axially symmetrical particles, the maximal value of $\Delta_{vh} = 3/4$ can be achieved with the condition

$$\mathrm{Re}(\alpha_1^*\alpha_2) = -\frac{1}{4}|\alpha_1|^2 - |\alpha_2|^2 \tag{12}$$

which, at real ϵ, is equivalent to

$$\alpha_1 = -2\alpha_2 \tag{13}$$

For nonabsorbing particles, the condition 13 leads to the equation

$$\epsilon = 1 - \frac{6}{3L_a + 1} \tag{14}$$

which gives $\epsilon = -5$ for thin rods or $\epsilon = -1/2$ for thin disks.

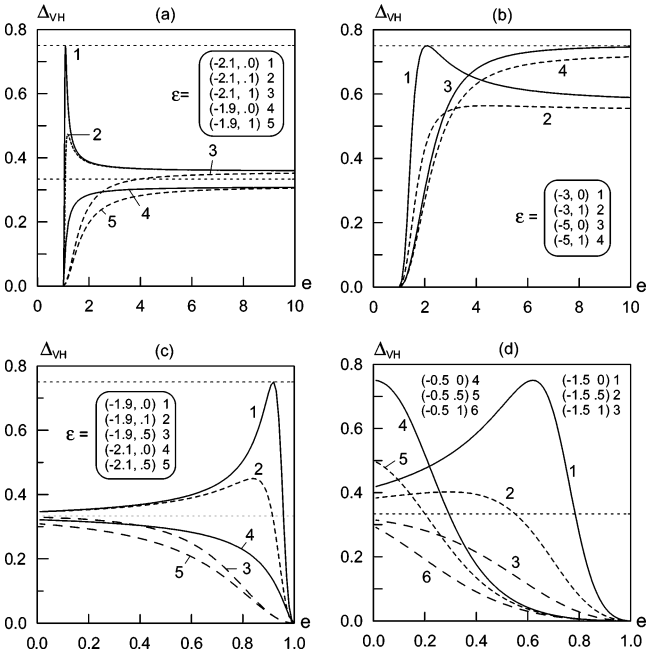

Figure 2. Dependence of the depolarization ratio Δ_{vh} on the axis ratio $e = a/b$ of prolate (a,b) and oblate (c,d) spheroids with various values of the relative dielectric permeability ϵ. The ϵ values are indicated in figures and were taken within and out of the fields A and B shown in Figure 1.

Figure 2 shows the dependence of the depolarization ratio on the axial ratio of Rayleigh spheroids. The calculations were performed for characteristic values of ϵ, which are within or out of regions A and B in Figure 1. Interestingly, at small deviations of the particle shape from the spherical shape ($e \approx 1$, $L_1 \approx 1/3$), eq 15 again leads to the plasmon resonance condition 11. Calculations for nonabsorbing particles (Figure 2a, curve 1) or for particles with small absorption (Figure 2a, curve 2) show that the condition 12, indeed, can be satisfied at small deviations from the spherical form, if $\mathrm{Re}\epsilon$ is slightly smaller than -2. It is a rather unexpected result because the maximal depolarization is usually assumed for extremely nonspherical particles such as thin needles or disks. With an increase in the particle substance absorption (Figure 2a, curve 3), the unusual resonant depolarization value near $e \approx 1$ disappears and all curves tend to a common limit, which is slightly greater than 1/3.

Curve 3 in Figure 2b illustrates the above-mentioned limit $\Delta_{vh} = 3/4$ ($\epsilon = -5$) for thin needles ($e \rightarrow \infty$). For the region $-5 < \mathrm{Re}\epsilon < -2$, this limit can be achieved at finite values of the axial ratio (see curve 1 in Figure 2b), whereas the depolarization ratios are smaller than 3/4 at $e \rightarrow \infty$. In all cases studied, the absorption of particle substance decreases the depolarization ratio (see dashed curves in Figures 2a−d).

Curves 1 and 2 in Figure 2c illustrate the unusual appearance of large depolarization by oblate particles with a small axial ratio when the dielectric permeability values are near plasmon the resonance (11) within the upper semicircle *A* in Figure 1 ($\mathrm{Re}\epsilon = -1.9$). Outside this semicircle ($\mathrm{Re}\epsilon = -2.1$, curves 4 and 5 in Figure 2c), the depolarization ratios are smaller than 1/3. Curve 4 in Figure 2d illustrates the theoretical limit $\Delta_{vh} = 3/4(\epsilon = -1/2)$ for thin disks ($e \rightarrow 0$), which decreases greatly with an increase in particle absorption (curves 5 and 6). Curves 1−3 in Figure 2d show the dependence of depolarization on the particle shape when the ϵ values are within region *A* in Figure 1 (curves 1 and 2, Figure 2d) or outside it (curve 3).

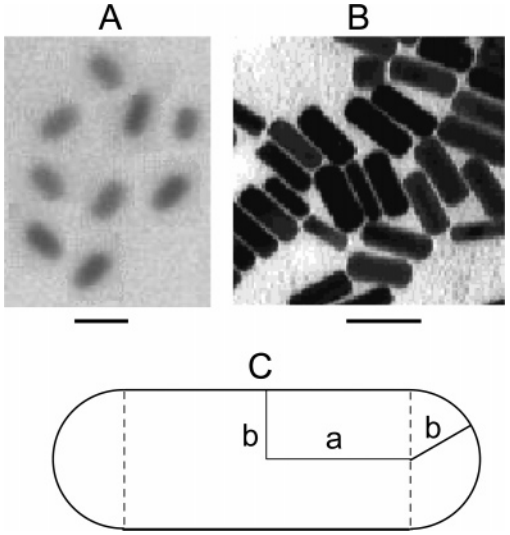

Figure 3. TEM images of gold NRs with plasmon resonance peaks at 655 nm (A) and 700 nm (B, after Nikoobakht and El-Sayed[13]). The s-cylinder model (C) is defined by the geometric sizes *a* and *b*. The scale bar is 50 nm.

The applicability of tensor eq 6 to modeling the light scattering depolarization of real systems is restricted by the spheroidal particle shape and by the small particle sizes. Rather than spheroids, the actual shape of experimental gold nanorods[12,13,21] can be better modeled by cylindrical rods with length $2a$ and semispherical ends of radius b (s-cylinder model,[15,16] Figure 3). The axial ratio of an s-cylinder is equal to $e = (a + b)/b$. To calculate the optical properties of such particles, we used the exact *T*-matrix method.[15] In our codes, the *T*-matrix elements are numerically calculated by the known formulas,[6] in which the spheroidal particle shape function $r(\vartheta)$ was replaced by the expression

$$r(z = \cos\vartheta) = \begin{cases} a[z + ((b/a)^2 + z^2 - 1)^{1/2}], & \mathrm{tg}\vartheta \le b/a \\ \dfrac{b}{(1 - z^2)^{1/2}}, & \mathrm{tg}\vartheta \ge b/a \end{cases} \tag{15}$$

The *T*-matrix of spheroids and s-cylinders was used to calculate the scattering matrix F_{ij} which relates the Stokes parameters (I_v, I_h, U, V)[6] of the incident and scattered light. The averaging of $\langle F_{ij} \rangle$ over random particle orientations was carried out as described in ref 24. The depolarization ratio Δ_{vh} is equal to the normalized scattering matrix element $\langle F_{12} \rangle / \langle F_{11} \rangle = \langle F_{vh} \rangle / \langle F_{vv} \rangle$. The orientationally averaged extinction and scattering cross-sections were calculated by analytical formulas involving the *T*-matrix trace and its quadratic form.[6,25]

3. Experimental Section

3.1. Preparation of Nanospheres and Nanorods. In our experimental protocol, the following reagents were used: tetrachloroauric acid (TCAA) (Aldrich), cetyltrimethylammonium bromide (CTAB) (Serva, Germany), sodium borohydride (Serva, Germany), silver nitrate (Reachem Co., Russia), ascorbic acid (Reachem, Russia), and tridistilled water. All glassware used was cleaned by 3:1 HCl/HNO_3 and was rinsed thoroughly in H_2O before use.

Gold nanospheres were prepared by the citrate reduction method.[26] The average diameters of particles (21, 29, and 46 nm) were determined by using the calibration curve "particle diameter vs extinction peak position."[26] These samples were designated NS-21, NS-29, and NS-46 according to their average

diameters. From dynamic light scattering measurements, the weight-average hydrodynamic diameters of samples were equal to $d_w = 23.5$, 26.5, and 45 nm, respectively.

Au NRs were synthesized according to the seed-mediated growth method[13] with minor modifications concerning the concentrations of some reagents and the reaction protocol. During seed formation, fine gold nanoparticles with diameters of a few nanometers were synthesized in the presence of CTAB. To this end, 1 mL of 0.1 M CTAB solution was mixed with 25 μL of 0.01 M TCAA. To this vigorously stirred mixture, 100 μL of freshly prepared 0.01 M ice-cold $NaBH_4$ solution was added. On addition of $NaBH_4$, the color of the seed solution turned from light yellow to brownish yellow. The seed solution was again stirred vigorously for 1 min.

At the second step, the growth solution was prepared first, by mixing a 9.5 mL of 0.1 M CTAB with a varying volume of 0.004 M $AgNO_3$ (from 50 μL to 250 μL, depending on the desired NR length). To this solution, 500 μL of 0.01 M TCAA and 100 μL of 0.0788 M ascorbic acid was added as quickly as possible with vigorous mixing. To the growth solution, 12 μL of seed solution (aged 10 min) was added. The total reaction time may take several hours, and the final solution color depends on the axial ratio of NRs. The description of the synthetic protocol, including temporal optical monitoring and centrifugation in the density gradient of glycerol, can be found elsewhere.[27] According to their long-wavelength peak positions, the NR samples were designated NR-655, NR-692, and NR-900.

3.2. Spectral and Polarization Measurements. The extinction spectra of sols were recorded with a Specord M 40 spectrophotometer (Carl Zeiss, Jena, Germany) by using standard 1-cm cuvettes. Along with the extinction spectra, we recorded differential light scattering spectra (DLSS) by using a special attachment to the Specord M 40 as described in our previous works.[28−30]

The average particle sizes and the depolarization ratio I_{vh}/I_{vv} were measured with a homemade device for dynamic light scattering (DLS) experiments.[31] The linearly polarized He−Ne laser light (vertical polarization with respect to the scattering plane) was scattered at 90° by colloids placed in a four-sided, 1-cm rectangular cuvette. The only modification was that we placed a polarizer before a multiplier operating in the photon counting mode. Therefore, by changing the analyzer orientation from horizontal ("h") to vertical, we could measure the depolarization ratio I_{vh}/I_{vv} as the corresponding ratio of the average number of counted photons. To estimate the instrumental light depolarization, we used a dilute suspension of polystyrene latex (average diameter of spherical particles, 100 ± 5 nm, Sigma, USA). For comparative experiments, the depolarization of NS-21, NS-29, and NS-46 gold nanospheres was also measured. We used DynaLS software[32] to convert the photocurrent autocorrelation function into the particle size distribution and the average particle diameters.

4. Results and Discussion

By using a modified T-matrix code,[15,24] we calculated the extinction $A(\lambda) = A_{abs}(\lambda) + A_{sca}(\lambda)$, integral scattering $A_{sca}(\lambda)$, and depolarization ratio $\Delta_{vh}(\lambda)$ spectra for randomly oriented spheroids and s-cylinders in water for particle thickness $2b = 5-40$ nm (step 5 nm) and axial ratios $e = 1-3$ (step 0.2), 4−10 (step 1).

The optical dielectric functions of gold NRs were obtained by the same procedure as in refs 15 and 24. Specifically, we assumed the interband contribution to be independent of the particle size; therefore, the size-corrected dielectric permittivity

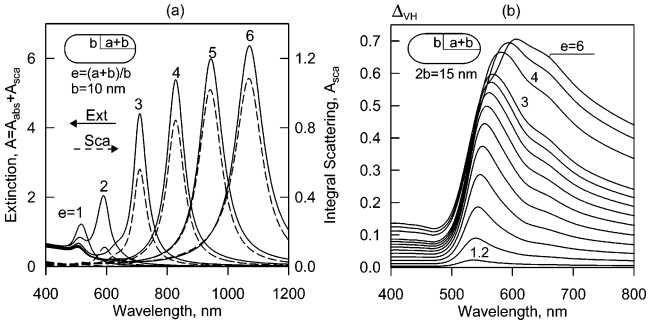

Figure 4. Depolarization ratio spectra $\Delta_{vh}(\lambda)$ calculated for randomly oriented gold s-cylinders with a thickness $2b = 15$ nm and an axis ratio $e = 1.2-3$ (step 0.2), 4−6 (step 1). The surrounding medium is water.

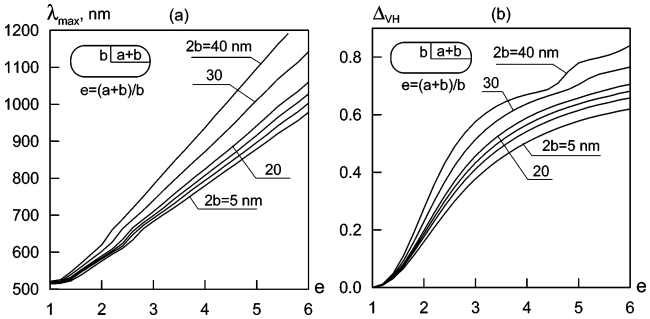

Figure 5. Dependence of the longitudinal plasmon resonance wavelength, λ_{max}, (a) and the depolarization ratio Δ_{vh} on the axis ratio of randomly oriented gold s-cylinders of various thicknesses $2b = 5-20$-(5), 30, and 40 nm. The Rayleigh approximation curves coincide with the bottom curves calculated for a particle thickness $2b = 5$ nm. The surrounding medium is water; the wavelength equals 632.8 nm (panel b).

can be expressed as $\epsilon_R = \epsilon_b(\lambda) + \Delta\epsilon(R_{ev},\lambda)$, where ϵ_b is the bulk value[33] and the correction $\Delta\epsilon(R_{ev},\lambda)$ accounts for an "isotropic" size-dependent contribution to the electron mean free path, according to refs 23 and 26.

Figure 4a shows an example for s-cylinders ($2b = 20$ and $e = 1-6$) in water. All spectra are normalized to our typical experimental conditions:[26] the gold concentration $c_g = 57$ μg/mL, and the cuvette thickness $l = 1$ cm. Figure 4b shows the depolarization ratio spectra $\Delta_{vh}(\lambda)$ calculated for gold s-cylinders with thickness $2b = 15$ nm and axial ratio $e = 1.2-3$ (step 0.2), 3−6 (step 1). It follows from these calculations that the depolarization ratio becomes greater than 1/3 in the red part of the spectrum even at moderate axial ratios $e > 2$. With an increase in the particle thickness, the depolarization spectra move to the red part of spectrum, but its general character corresponds to the data of Figure 4b.

Figure 5a shows the dependence of the long-wavelength peak position on the axial ratio at different thicknesses of randomly oriented gold s-cylinders in water. The Rayleigh approximation curve (not shown) coincides with the exact T-matrix calculation for a thickness $2b = 5$ nm and gives admissible accuracy up to a particle thickness $2b = 10-20$ nm. Figure 5b shows the dependences $\Delta_{vh}(e)$ calculated for the same model as in Figure 5a at a He−Ne laser wavelength $\lambda = 632.8$ nm. For a typical gold NR thickness of 15 nm,[13] the Rayleigh approximation gives underestimated data. Analogous results have been obtained for gold spheroids. For particles of both types, the data on the extinction and scattering spectra are close to the data of refs 15 and 16 and are not shown here. The scattering contribution to the total extinction exceeds 10% only for NRs with thicknesses greater than 20 nm, whereas for smaller NRs the extinction is

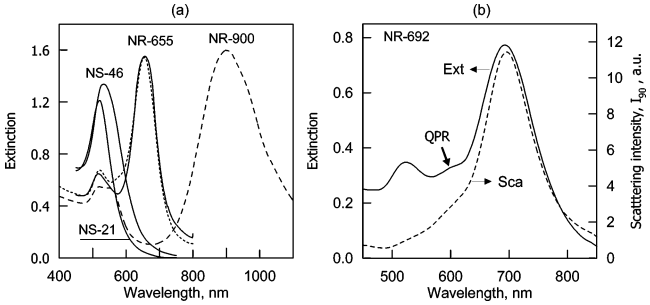

Figure 6. (a) Extinction spectra of nanospheres NS-21 and NS-46 and nanorods NR-655, freshly prepared (solid curve) and one month after preparation (dotted curve), and NR-900 (dashed curve). (b) Extinction (solid line) and scattering (dashed line) spectra of nanorods NR-692 (b). A spectral shoulder near 600 nm is indicated ("quadrupole resonance," QPR). For nanospheres, the gold concentration is 57 μg/mL and the optical thickness is 1 cm. The spectra of nanorods are normalized arbitrarily for graphic representation.

determined basically by absorption, which obeys dipolar approximation.[34]

Figure 6a shows the experimental extinction spectra of NS-21 and NS-46 nanospheres, NR-900 nanorods, and the sample NR-655 (freshly prepared; differential centrifugation in the density gradient of glycerol; solid curve) and for the same sample a month after (dashed curve; both spectra were normalized to the same maximum). Minor spectral differences of these spectra near 580 nm can be attributed to possible particle aggregation. The extinction and differential light scattering spectra of the NR-692 sample (Figure 6b) have coincident long-wavelength plasmon resonance,[13,14] corresponding to the longitudinal excitation of NRs along the major axis. We also note an extinction shoulder near 600 nm, which is absent in the scattering spectra. A comparison with data of Figure 5a suggests that this extinction shoulder can be related to lateral aggregation of NRs and to the quadrupole resonance. Theoretical quadrupole extinction and scattering resonances have been predicted for gold and silver nanorods (spheroids, s-cylinders, prisms),[15,35,36] as well as for oblate silver spheroids.[37] The quadrupole resonance can be excited only by the TM incident wave mode and it is maximal for an orientation angle of 54° between the particle axis and the incident light direction.[15,36] An appreciable contribution of the quadrupole resonance to the extinction spectra of randomly oriented gold NRs may be observed only for the equivolume particle diameters greater than 50−80 nm. Quite recently, Millstone et al. (ref 38) observed a quadrupole plasmon resonance for a colloidal solution of gold nanoprisms.

The experimental depolarization ratios Δ_{vh} are listed in Table 1. For polystyrene spheres, a small value $\Delta_{vh} \simeq 0.0048$ is in agreement with the expected zero depolarization ratio of ideal dielectric spheres. In addition, this small depolarization ratio indicates a negligible depolarization contribution caused by the optical elements of our setup. The depolarization ratio of gold nanospheres increases in the order NS-21 < NS-29 < NS-46 from 0.07 to 0.16, which can be explained by the previously reported[26,39] increase in the ellipticity of large particles synthesized by the citrate method. The average values of the axial ratio of nanospheres were evaluated by using Figure 1 of ref 39 and by the formula in ref 26 which relates the axial ratio to the equivolume diameter, d_{ev}, of particles:

$$e = 1 + \frac{d_{ev}}{p} \qquad (16)$$

where d_{ev} is expressed in nm and the constant $p \simeq 40$. Table 1 gives the arithmetic average of the above estimations. The theoretical values of the depolarization ratio are listed in the last column and are in good agreement with experimental measurements.

TABLE 1: Extinction Plasmon Resonance Wavelengths and the Light Scattering Depolarization Ratios Measured at 632.8 nm for the Gold Nanospheres NS-21, NS-29, and NS-46 and for the Nanorods NR-655, NR-692, and NR-900

sample	λ_1, nm	λ_2, nm	e	Δ_{vh}^{exp}	Δ_{vh}^{calc}
NS-21[a]	521.0		1.4	0.07 ± 0.01[b]	0.036
NS-29	525.5		1.6	0.09 ± 0.002	0.078
NS-46	533.5		1.9	0.16 ± 0.01	0.15
NR-655	519.2	654.5	2.6	0.353 ± 0.003	0.35
NR-692	524.1	692.4	3.0	0.294 ± 0.003	0.41
NR-900	520, 548[c]	900	4.9	0.370 ± 0.004	0.62
				0.48 ± 0.05[d]	0.46[d]

[a] The single resonance wavelength is given for nanospheres. [b] Standard deviations are calculated for 5 parallel runs. [c] Two plasmon bands are observed for this sample. [d] Measurements and calculations at 740 nm.

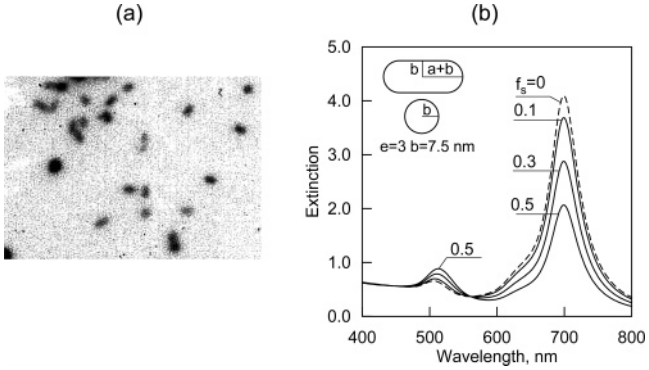

Figure 7. TEM image of NR-692 sample (a) and the extinction spectra calculated for a mixture of spheres and randomly oriented nanorods (b). The volume fraction of spheres $f_s = 0$, 0.1, 0.3, and 0.5. Note the presence of spherical particles in the NR-692 sample.

As our protocol of NR synthesis is analogous to that of ref 13, possible variations in the NR thickness should be within the range $2b = 10-20$ nm. This estimation agrees with the average TEM value $2b = 16$ nm. By using the long-wavelength resonance position and the data of Figure 4a, we found the possible aspect ratios of NR-655 to be within the range $e = 2.5-2.7$ (the average value $e = 2.6$ gives the resonance wavelength $\lambda_2 = 656$ nm). From TEM images, the average aspect ratio of NR-655 is equal to 2.5, in good agreement with spectral estimation. Finally, by using Figure 4b and taking into account the geometrical parameters $2b = 16$ nm and $e = 2.5$, we get the theoretical depolarization ratio $\Delta_{vh}^{calc} = 0.37$, which is in excellent agreement with the measured value $\Delta_{vh}^{exp} = 0.36$.

For the NR-692 sample, analogous estimations lead to the possible aspect ratio range $e = 2.8-3.2$ (the average value $e = 2.8$ gives the resonance wavelength $\lambda_2 = 700$ nm). The corresponding theoretical depolarization ratios $\Delta_{vh}^{calc} = 0.38-0.44$ are noticeably higher than the experimental value $\Delta_{vh}^{exp} = 0.29$. In addition, the theoretical ratio of the plasmon resonance peaks $A(\lambda_2)/A(\lambda_1) \simeq A(700)/A(508) \simeq 6$ is three times higher than the measured ratio $A(\lambda_2)/A(\lambda_1) \simeq 2$. There are several causes for these discrepancies, including the particle polydispersity and shape polymorphism. In particular, the low depolarization ratio and the decrease in the longitudinal resonance quality can be explained by the presence of spherical particles, which are clearly seen in the TEM images (Figure 7a). This suggestion is in agreement with the fact that the experimental resonance peak $\lambda_1 = 524$ nm is markedly higher than the theoretical short-

wavelength peak position of nanorods (508 nm). It should be emphasized that the spherical particles may change the value and position of the short-wavelength resonance but not the long-wavelength resonance. That is why the above estimations of the particle axial ratio can be considered quite reliable because they were based on the long-wavelength peak position. We calculated extinction spectra by using the simplest model of a two-fractions mixture consisting of spheres with radius b and s-cylinders with an axis ratio $e = (a + b)/b$ (Figure 7b). The volume fraction of nanospheres was varied from 0.1 to 0.5. This simple model does allow one to explain the significant decrease in the plasmon resonance peak ratio (from 6 to 2), and the decrease in the depolarization ratio, if the volume fraction of nanospheres and NRs are taken to be close. However, for a more careful comparison between experimental and calculated spectra, one needs explicit data on the particle size and shape distribution. For example, the lateral aggregation of nonspherical particles can also result in a decrease in the depolarization ratio. On the other hand, aggregation of spherical particles may enhance the depolarization, as it has been shown for fractal clusters of soot[40] and colloidal gold.[41]

For NR-900 particles, the long-wavelength resonance position gives an average aspect ratio of 4.9, which corresponds to the theoretical depolarization ratio $\Delta_{vh}^{calc} = 0.62$ at $\lambda = 632.8$ nm. As in the case of the NR-692 sample, the measured value $\Delta_{vh} = 0.37$ is markedly smaller. We have already discussed the possible causes for such discrepancies. Additionally, in this case, the probing wavelength $\lambda = 632.8$ nm gets into an unfavorable region where light scattering from NR-900 nanorods is extremely small (the resonance wavelength is about 900 nm). We attempted to measure the depolarization ratio spectrum within the range 650−750 by using the same attachment to the Specord M-40 spectrophotometer as described in the Experimental Section. The lower limit of the above spectral region was restricted by the small scattering intensity, and the upper limit was restricted by the quality of available polaroids. As the incident light intensity was rather small, the scattered light was recorded without an analyzer. The measured value $\Delta_u = I_{hu}/I_{vu}$ was recalculated as Δ_{vh} by the relationship[4]

$$\Delta_{vh} = \frac{\Delta_U}{2 - \Delta_U} \tag{17}$$

Measurements of reference samples (polystyrene latex L-100 and specially prepared NS-90 gold nanospheres) with the known depolarization showed that our light scattering attachment gave an instrumental depolarization of about 0.2 within the spectral range 650−750 nm. Therefore, the actual depolarization $\Delta_{vh}(\lambda = 740) = 0.48$ (Table 1) was obtained by subtraction of the instrumental contribution from the measured value. Of course, such an estimate is not reliable. Nevertheless, it agrees well with the theoretical value $\Delta_{vh}^{calc}(\lambda = 740) = 0.46$ obtained for the axial particle ratio of 4.9. For smaller wavelengths, the agreement between calculated and measured (by the subtraction recipe) depolarization ratios was unsatisfactory.

5. Conclusion

Our analysis showed that the depolarization ratios $\Delta_{vh} > 1/3$ can be observed for axial particles for which relative dielectric permeability lies in the left upper quadrant of the complex ϵ plane. In particular, for thin disks and needles, the corresponding ϵ regions are presented in Figure 1. The maximum possible value of $\Delta_{vh} = 3/4$ may be observed for particles possessing a polarizability tensor that obeys eq 12. An unexpected theoretical result is that condition 12 and the maximal value of $\Delta_{vh} = 3/4$ can be obtained at small deviations of the particle shape from the sphere (Figure 2), provided that the particle absorption is small and the condition $\mathrm{Re}(\epsilon) = -2 + \delta(\delta \rightarrow 0)$ is satisfied. The plasmon-resonant particles are objects for which high (>1/3) depolarization ratios can really be observed. Calculations of the depolarization ratio spectra for gold spheroids and s-cylinders showed strong depolarization of the scattered light in the red part of the spectrum. Experimental depolarization ratios for "sphere-like" particles NS-21, 29, and 46 and for NR-655 and NR-900 nanorods are in good agreement with theoretical calculations based on the average axial ratios found from the extinction spectra and TEM data. We have measured the depolarization ratios $\Delta_{vh} = 0.36$ (NR-655, $\lambda = 632.8$ nm) and 0.48 (NR-900, $\lambda = 740$ nm), which are markedly higher than the theoretical limit 1/3 of dielectric anistropic scatterers. The underestimated depolarization and plasmon resonance peak ratios of NR-692 nanorods can be explained by the presence of spherical and, possibly, aggregated structures that contribute to the VV scattering intensity but not to VH scattering.

For small nanoparticles (the average size is less than 20 nm) the scattering efficiency is too small in comparison with dominant adsorption, while for 40-nm particles the contribution of scattering to the total extinction is about 60%. Thus, the measurements of depolarization ratio for such particles can give additional useful information for plasmon resonant particle characterization and their potential applications. To make this conjecture clear, let us consider shortly the following experimental example (a more detailed consideration will be published separately). As it has been shown in section 4, the depolarization ratio of citrate-synthesized gold nanospheres increases in the order NS-21 < NS-29 < NS-46 from 0.07 to 0.16. The significant depolarization by citrate spherical particles is consistent with reported[26,39] deviations of the citrate particle shape from spherical one. However, we have prepared also NS-90 gold nanospheres by using a noncitrate reduction protocol. The depolarization ratio of NS-90 colloid was close to 0.1, which was essentially smaller than the value 0.16 of NS-46 particles. Moreover, NS-90 sample falls out the above rule Δ_{vh}(NS-21) < Δ_{vh}(NS-29) < Δ_{vh}(NS-46). We suggested that the NS-90 nanospheres have an improved spherical shape as compared with usual citrate gold particles. This suggestion was confirmed by TEM images.

Another potential application of light scattering depolarization is related to the optical monitoring of biospecific molecular binding on a nanoparticle surface.[42,43] For instance, it has been shown recently[21] that gold nanorods can be considered as novel plasmon-based orientation sensors for polarized single-particle microscopy. These potentialities are due to strong polarization of light scattered by a gold nanorods.

Acknowledgment. This work was partly supported by grants from RFBR (nos. 05-02-16776a and 04-04-48224a). B.N.K. was supported by a grant from BRHE Annex BF4M06 Y2-B-06-08. N.G.K. was partially supported by grant nos. 01.2003.15221 and NSH-25.2003.2. We thank D. N. Tychinin (IBPPM RAS) for help in preparation of the manuscript.

References and Notes

(1) Rayleigh, D. W. *Philos. Mag.* S. 5. **1871**, *41*(107), 274.

(2) Rayleigh, D. W. *Philos. Mag.* S. 5. **1897**, *44*, 28.

(3) van de Hulst, H. C. *Light Scattering by Small Particles*; Wiley: New York, 1957.

(4) Kerker, M. *The Scattering of Light and Other Electromagnetic Radiation*; Academic Press: New York, 1969.

(5) Bohren, C. F.; Huffman, D. R. *Absorption and Scattering of Light by Small Particles*; John Wiley & Sons: New York, 1983.
(6) Mishchenko, M. I.; Travis, L. D.; Lacis, A. A. *Scattering, Absorption, and Emission of Light by Small Particles*; Cambridge University Press: Cambridge, 2002.
(7) Heller, W.; Nakagaki, M. *J. Chem. Phys*. **1974**, *61*, 3619.
(8) Mehta, R. V.; Shah, H. S.; Desai, J. N. *J. Colloid Interface Sci*. **1971**, *36*, 80.
(9) Ravey, J.-C. *J. Colloid Interface Sci*. **1976**, *56*, 540.
(10) Ravey, J.-C. *Eur. Polym. J*. **1972**, *8*, 937; Ravey, J.-C. *Eur. Polym. J*. **1973**, *9*, 47; Ravey, J.-C. *Eur. Polym. J*. **1973**, *9*, 57.
(11) Van der Zande, B. M. I.; Böhmer, M. R.; Fokkink, L. G. J.; Schönenberger, C. *Langmuir* **2000**, *16*, 451.
(12) Jana, N. R.; Gearheart, L.; Murphy, C. J. *Adv. Mater.* **2001**, *13*, 1389.
(13) Nikoobakht, B.; El-Sayed, M. A. *Chem. Mater*. **2003**, *15*, 1957.
(14) Link S.; El-Sayed, M. A. *Annu.* Rev. Phys. Chem. **2003**, *54*, 331.
(15) Khlebtsov, N. G.; Trachuk, L. A.; Melnikov, A. G. *Opt. Spectrosc.* **2004**, *97*, 105.
(16) Khlebtsov, N. G.; Trachuk, L. A.; Melnikov, A. G. *Opt. Spectrosc.* **2005**, *98*, 82.
(17) Parak, W. J.; Gerion, D.; Pellegrino, T.; Zanchet, D.; Micheel, C.; Williams, S. C.; Boudreau, R.; Le Gros, M. A.; Larabell C. A.; Alivisatos, A. P. *Nanotechnology* **2003**, *14*, R15.
(18) Niemeyer, C. M.; Mirkin, C. A.; Eds. *Nanobiotechnology: Concepts, Applications, and Perspectives*; Wiley-VCH: Weinheim, 2004.
(19) Chang, J.-Y.; Wu, H.; Chen, H.; Ling, Y.-C.; Tan, W. *Chem. Commun*. **2005**, *8*, 1092.
(20) Bauer, L. A.; Birenbaum, N. S.; Meyer, G. J. *Mater. Chem*. **2004**, *14*, 517.
(21) Sönnichsen, C.; Alivisatos, A. P. *Nano. Lett*. **2005**, *5*, 301.
(22) Berestetsky, V. B.; Lifshits E. M.; Pitaevsky, L. P. *Quantum Electrodynamics (Course of Theoretical Physics, 4)*; Pergamon: Oxford, UK, 1982.
(23) Coronado, E. A.; Schatz G. C. *J. Chem. Phys.* **2003**, *119*, 3926.
(24) Khlebtsov, N. G.; Melnikov, A. G. *Opt. Spectrosc.* **1995**, *79*, 605.
(25) Khlebtsov, N. G. *Appl. Opt*. **1992**, *31*, 5359.
(26) Khlebtsov, N. G.; Bogatyrev, V. A.; Dykman, L. A.; Melnikov, A. G. *J. Colloid Interface Sci.* **1996**, *180*, 436.
(27) Alekseeva, A. V.; Bogatyrev, V. A.; Trachuk, L. A.; Khlebtsov, N. G. *Proc. SPIE* **2005**, *5772*.
(28) Bogatyrev, V. A.; Dykman L. A.; Krasnov, Ya. M.; Plotnikov, V. K.; Khlebtsov, N. G. *Colloid J*. **2002**, *64*, 671.
(29) Khlebtsov, N. G.; Bogatyrev, V. A.; Dykman, L. A.; Khlebtsov, B. N.; Krasnov, Ya. M. *J. Quant. Spectrosc. Radiat. Transfer* **2004**, *89*, 133.
(30) Bogatyrev, V. A.; Dykman, L. A.; Khlebtsov, B. N; Khlebtsov, N. G. *Opt. Spectrosc*. **2004**, *94*, 161.
(31) Khlebtsov, B. N.; Chumakov, E. M.; Semyonov, S. V.; Chumakov, M. I.; Khlebtsov, N. G. *Proc. SPIE* **2004**, *5475*, 12.
(32) URL: http://www.photocor.com; http://www.protein-solutions.com
(33) Johnson, P. B.; Christy, R. W. *Phys. Rev. B* **1972**, *6*, 4370.
(34) Gans, R. *Ann. Phys.* **1912**, *37*, 881.
(35) Khlebtsov, N. G.; Khlebtsov B. N.; Melnikov A. G. *11th International Conference on Surface and Colloid Science (IACIS 2003, Abstracts)*, Iguassu Falls, Brazil, 2003, p 34.
(36) Khlebtsov, N. G.; Trachuk L. A.; Melnikov, A. G. *Proc. SPIE* **2004**, *5475*, 1.
(37) Kelly, K. L.; Coronado, E.; Zhao, L. L.; Schatz, G. C. *J. Phys. Chem. B* **2003**, *107*, 668.
(38) Millstone, J. E.; Park, S.; Qin, L.; Schatz, G. C.; Mirkin, C. A. *J. Am. Chem. Soc.* **2005**, *127*, 5312.
(39) Brown, K. R.; Walter, D. G.; Natan, M. J. *Chem. Mater*. **2000**, *12*, 306.
(40) Lu, N.; Sorensen, C. M. *Phys. Rev. E* **1994**, *50*, 3109.
(41) Lin, M. Y.; Lindsay, H. M.; Weitz, D. A.; Ball, R. C.; Klein, R.; Meakin, P. *Proc. R. Soc. London Ser. A* **1989**, *423*, 71.
(42) Stuart, D. A.; Haes, A. J.; Yonzon, C. R.; Hicks, E. M.; Van Duyne, R. P. *IEE Proc.-Nanobiotechnol.* **2005**, *152*, 13.
(43) P'erez-Juste, J.; Pastoriza-Santos, I.; Liz-Marz'an, L. M.; Mulvaney, P. *Coord. Chem. Rev.* **2005**, doi:10.1016/j.ccr.2005.01.030.